A 60 kb/s–10 Mb/s Adaptive Frequency Hopping Transceiver for Interference-Resilient Body Channel Communication

Namjun Cho, *Student Member, IEEE*, Long Yan, *Student Member, IEEE*, Joonsung Bae, *Student Member, IEEE*, and Hoi-Jun Yoo, *Fellow, IEEE*

***Abstract*—An interference-resilient 60 kb/s–10 Mb/s body channel transceiver using the human body as a signal transmission medium is designed for multimedia and medical data transaction in body-area network. The body antenna effect which interferes with signals in the human body channel is examined. The body-induced interferences degrade the SIR of the signal to −22 dB in the worst case. In order to overcome the body antenna effect, a 4-channel adaptive frequency hopping scheme using the 30–120 MHz band is introduced to the body channel transceiver. A direct-switching modulator using dual frequency synthesizers and a DLL-based demodulator are proposed for 10 Mb/s FSK and the 4.2 μs hopping time. The transceiver fabricated with 0.18 μm CMOS withstands −28 dB SIR and its operating distance is over 1.8 m with −25 dB SIR. Its energy consumption is 0.37 nJ/b with −65 dBm sensitivity.**

***Index Terms*—Adaptive frequency hopping, body antenna effect, body area network, body channel communication.**

I. Introduction

RECENTLY, the IEEE 802.15 Task Group 6 (TG 6) has been organized to standardize the frequency band and the protocols of medical and multimedia communications around a human body [1]. The existing WPAN standards such as IEEE 802.15.4 and 4a proved inefficient for wireless body area network (WBAN), and this mandates a new standard. For example, GHz bands for Zigbee or UWB suffer huge propagation loss through the human body. A recent experiment [2] shows that the path loss (PL) of the UWB signal around a body can be expressed as

$$PL(\mathrm{dB}) = PL_0 + 10n\log\left(\frac{d}{d_0}\right), \quad n = 6 \qquad (1)$$

where d_0 is the reference distance, and PL_0 is the path loss at d_0. n is the path loss exponent which indicates the dependency of the power attenuation amount upon the distance. Compared with free space or the case where $n = 3$, more than 30 dB/dec path loss near the body is expected due to the high energy absorption of the human tissue. In addition, the WPAN channel characteristics such as the path loss and the delay spread are highly dependant on the locations in a body [3]. Since most WPAN transceivers are developed to provide at least 10–100 m communication range, their output power and sensitivity are not optimized for the body area which needs to cover only $<$ 3 m. Moreover, the long distance coverage of the WPAN makes it difficult to isolate the channel from adjacent networks. Recently, the body channel communication (BCC), which uses the human body as a communication channel, has been studied as a solution to converge health care and multimedia applications on the human body [4]. Since the signals are transmitted between on-body transceivers through the conductive human tissue with the floated grounds as the capacitive return path, the BCC can utilize low frequency bands under 150 MHz without large antennas. This reduces power consumption and size of the transceiver substantially. In addition, the BCC is based on the near-field coupling mechanism where the path loss exponent (n) is 3, leading to 30 dB/dec enhancement compared with the WPAN channel around a body where $n = 6$ [5]. Moreover, the transmitter does not need to drive a low impedance antenna which is a major source of the power consumption in wireless communication. By taking advantages of these features, recent body channel transceivers achieved 10 times more energy efficient data transmission than conventional short range radios [6], [7]. However, their communication reliability is not satisfactory because the received signal through a body is often strongly contaminated by external interferences. The main cause of the signal corruption is the human body antenna effect. As shown in Fig. 1, the human body under electromagnetic fields behaves as an antenna with its resonance frequency determined by the wavelength (λ) equal to twice of the human height. In case that the body is grounded, the resonance wavelength λ is equal to four times of the height due to the mirror effect [8]. This means that the body resonance may occur at different frequencies, depending on various environmental conditions. Since the human body is a lossy conductor with its conductance value of 1 S/m and has a complex shape, its resonance peaking is not sharp but broadly distributed [9]. Therefore, the human body operates as a wideband antenna in 40–400 MHz frequency range.

The body antenna effect can inject various radio signals into the human body, and degrades the SIR of the signal significantly. Fig. 2 shows the in-band interferences coupled to a body

Manuscript received April 13, 2008; revised November 28, 2008. Current version published February 25, 2009.

The authors are with the Department of Electrical Engineering and Computer Science, Korea Advanced Institute of Science and Technology (KAIST), Daejeon 305-701, Korea (e-mail: buzm@eeinfo.kaist.ac.kr; yanlong@ee.kaist.ac.kr; joonsung@ee.kaist.ac.kr; hjyoo@ee.kaist.ac.kr).

Color versions of one or more of the figures in this paper are available online at http://ieeexplore.ieee.org.

Digital Object Identifier 10.1109/JSSC.2008.2012328

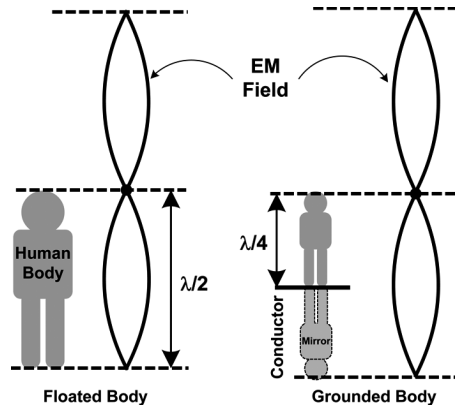

Fig. 1. Human body resonance under electromagnetic fields.

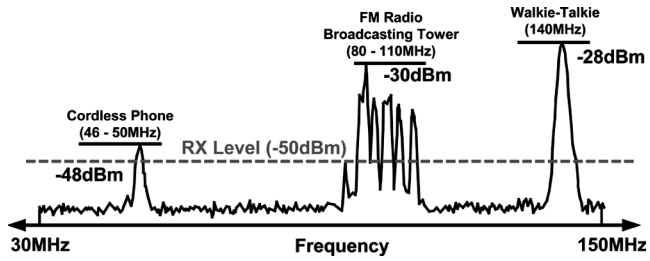

Fig. 2. Measured in-band interferences due to the body antenna effect.

channel receiver coming from wireless sources nearby. In order to get the measured data, a spectrum analyzer is connected to the human subject using a coaxial cable and a circular electrode attached to the left hand [5]. All measurements are performed outdoors, 1 km away from the radio broadcasting tower, and the possible interferences such as the cordless phone and the walkie-talkie signals are generated intentionally. Note that a 1.5 V_{P-P} signal at the TX side is attenuated to -50 dBm through the 1.8 m body channel in the measured frequency range [5]. Within the FM radio band of 88–108 MHz, a number of interference signals exist through the air, and their levels are up to -30 dBm, degrading the SIR of BCC down to -20 dB. When a walkie-talkie is held by a BCC user, the power of the injected signal becomes larger, so that the SIR degrades to -22 dB. For the stable BCC, robustness to SIR is more important than to SNR.

In this paper, a body channel transceiver is presented to handle in-band interferences higher than -20 dBm. More specifically, an adaptive frequency hopping (AFH) technique is introduced to improve SIR. The AFH is a variant of frequency hopping spread spectrum to improve resistance to in-band interferences by excluding the corrupted frequencies from the hop set [10]. Since only clean channels are assigned for communication, the AFH can avoid the interference with the

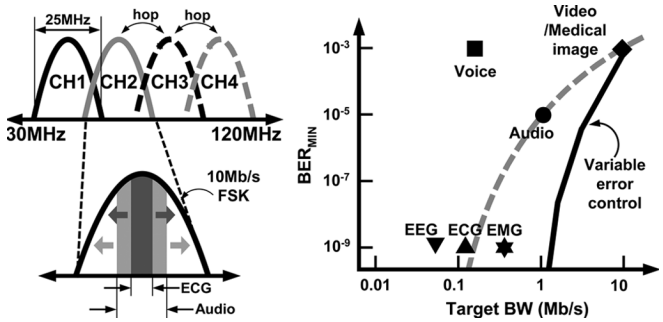

Fig. 3. Channel utilization for AFH BCC.

reduced number of hopping channels. This enables larger signal bandwidths and the higher data rates than normal spread spectrum schemes for a given spectrum resource. By adopting the AFH, the proposed transceiver can achieve 28 dB of interference rejection while providing a 10 Mb/s data rate. A direct-switching modulator using dual frequency synthesizers supports the AFH with a short hopping time of 4.2 μs. A DLL-based demodulator enables 10 Mb/s FSK signaling by reducing the transition jitter by half. The data rate and the BER of the transceiver are also highly scalable, allowing the BCC system to be applied to various body-area services.

This paper will explain in detail how to resolve the interference problems which are the main obstacle for the practical usage of the BCC. Section II describes the system overview including the channel utilization and the transceiver architecture for AFH. The detail design of the body channel transceiver and its measurements are discussed in Sections III and IV, respectively. Finally, Section V concludes this paper.

II. System Overview

A. Channel Utilization

Fig. 3 shows the frequency plan for AFH BCC. According to the channel analysis considering the path loss through the human body and the emission power radiated from the human body, the 30–120 MHz band is found to give the highest SNR [5]. This 90 MHz band is divided into 4 channels to perform the AFH. Each channel of the 25 MHz bandwidth can support a maximum data rate of 10 Mb/s, enabling multimedia transmission. Since the number of the available channels is just 4, conventional direct sequence and frequency hopping spread spectrums may provide just 6 dB of processing gain [11]. However, with the AFH, every channel status is continuously monitored and only the clean channels are used for the selective frequency hopping to increase the processing gain. The packet throughputs of the regular hopping and the AFH using the 4 channels are simplified [12] as shown in (2) at the bottom of the page, where

$$\begin{cases} FH\ Throughput = \frac{TX\ Packets}{s} \cdot \left(\frac{4-N_B}{4}\right) \\ AFH\ Throughput = \frac{TX\ Packets}{s} \cdot \left(\frac{N_G - P_B N_G}{N_G + P_B N_G P_G N_B}\right) \end{cases}. \tag{2}$$

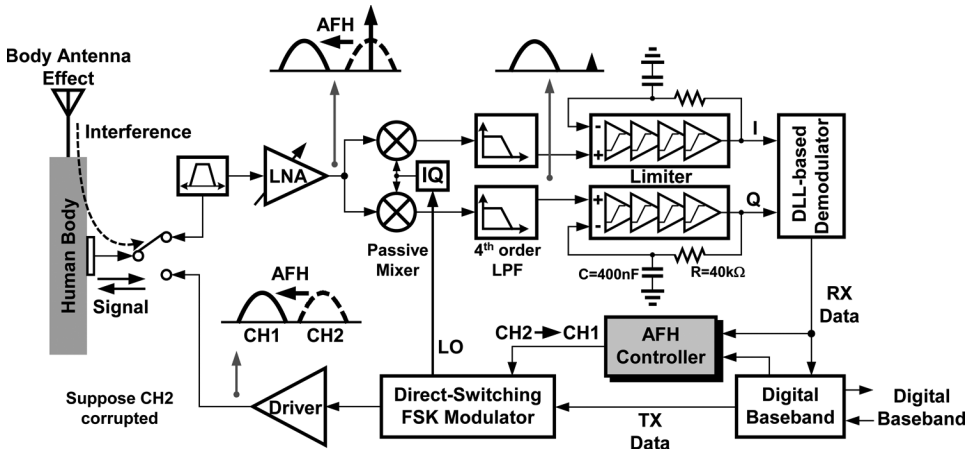

Fig. 4. Transceiver architecture.

N_G and N_B are the numbers of good and bad channels, respectively. P_B is the probability of a good channel erroneously accepted as a bad one, and P_G is vice versa. As the number of bad channels attacked by external interferences increases, the throughput of the regular FH decreases linearly. However, the AFH can maintain the maximum throughput as long as there is no false evaluation of the channel $(P_B = P_G = 0)$ and at least one channel remains clean $(N_G > 0)$. Even when all channels are corrupted by interferences $(N_G = 0)$, the throughput can be sustained by the channel showing the highest SIR. On average, more than 10 dB improvement in the interference rejection is achieved with the 4 channel AFH scheme, compared to a regular frequency hopping.

In order to amalgamate consumer electronics with health care functions in a body area network, BCC should support wide range of quality-of-service (QoS) in terms of data rate and BER as shown in Fig. 3. Interestingly, the relation between the two parameters is not random, but positively correlated [1]. To transfer medical information such as ECG and EMG, high reliability of 10^{-9} BER is required. However, the data rate is sufficient with around 500 kb/s. For multimedia data, relatively low BER of 10^{-3} is allowed while the transmission rate has to be up to 10 Mb/s. Therefore, a variable error control is presented for the channel coding, where the actual data rate through the body is fixed to the maximum 10 Mb/s regardless of the data type and the excess bandwidth in the low rate transmission is reserved for error control coding. For example, when the videos or medical images need to be transmitted, the entire 10 Mb/s bandwidth is utilized. And for the audio data requiring just 1 Mb/s, the excess 9 Mb/s bandwidth is used for the error control, making both the data rate and the BER scalable. Within each channel, a wideband FSK is selected as the modulation scheme with 10 MHz frequency separation. Since the FSK carries data on its zero crossings, it is robust against amplitude distortion due to the frequency dependent loss of the body channel [5].

B. Transceiver Architecture for AFH

The overall architecture of the AFH BCC transceiver is shown in Fig. 4. The front-end design is optimized for the 10 Mb/s BFSK and the fast hopping speed. The receive chain adopts the direct conversion scheme. It is because the common issues of the direct conversion due to the LO self-mixing and I/Q mismatch can be ignored due to its relatively low operating frequency of < 150 MHz. The high pass filter required to cancel the DC offset and flicker noise does not disturb the wideband FSK signal through the human body, so direct conversion is most efficient for the highly integrated, low-noise body channel receiver. In this architecture, a single electrode is adopted for the simple interface with the human body [6]. The incoming signal through the body and interferences from external sources due to the body antenna effect are amplified in the LNA together and down-converted to zero-IF by passive I/Q mixers. The following fourth-order Salen-Key filter with 9 dB voltage gain and 10 MHz cut-off frequency amplifies the wanted signal further and removes out-of-channel interferences. The filtered based-band signal is digitized through the limiter which is a direct-coupled cascade of five differential amplifiers. Due to the high gain of the limiter, the duty cycle of its output is very sensitive to the DC-offset added by the mixer and the baseband filter. The low-pass-feedback formed by the R (40 kΩ) and C (400 nF) can reject up to 400 mV DC-offset, maintaining 48% duty cycle. The high pass filtering also removes the flicker noise accompanied with the input signal. A DLL-based demodulator is incorporated to demodulate the 10 Mb/s FSK signal in the zero-IF. It can reduce the transition jitter of the RX data by half. In the transmit path, the binary data from the digital base band is modulated with 10 Mb/s FSK and applied to the human skin through the single electrode. The frequency switching time in the AFH system is reduced to 4.2 μs by a direct-switching modulator to minimize the acquisition overhead of the hopping transceiver. The detailed operation of the proposed building blocks will be explained in the next section.

The AFH controller placed between the transmitter and receiver chains is the key building block for AFH. Fig. 5 describes its operation with a flowchart. Initially, the controller assumes that there exists no interference and all of the channels are used for frequency hopping. During the communication interval $(\mathrm{T_I})$, the transceivers transmit and receive packets, hopping their channels with the hopping period $(\mathrm{T_H})$. The controller continuously monitors the status of each channel by calculating its packet success ratio (PSR). In order to decide suc-

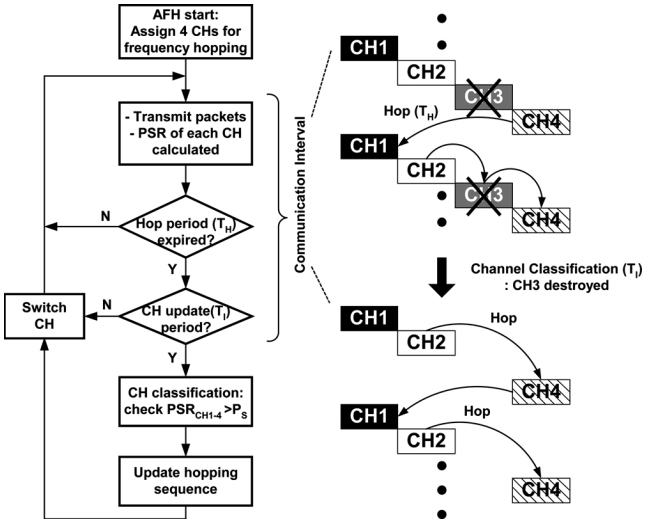

Fig. 5. AFH operation.

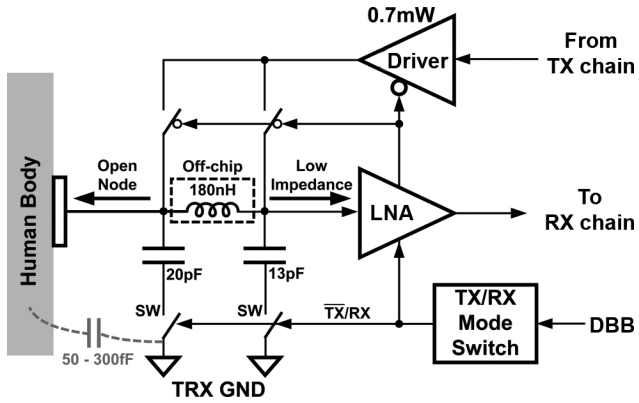

Fig. 6. Front-end interface to human body.

cess of each packet transmission, following 2 criteria are used. First, when the packet requiring acknowledgement from the receiver is transmitted but there is no response, the packet fails to be transmitted. Second, although the packet reception is detected by the physical layer, the CRC-check of the RX bit stream yields incorrect value. Then the packet error occurs. The controller assumes that all of the packet errors result from the bad channel quality. After sufficient number of packet transactions ($\mathrm{T_I}$), the channel classification is performed and only the clean channels which have PSRs larger than the pre-defined threshold ($\mathrm{P_S}$) are selected for the next communication. By repeating this sequence, the interferences are avoided from the channel automatically, and then removed through the base band filter. As expected, the performance of the AFH is highly affected by $\mathrm{T_H}$, $\mathrm{T_I}$, and $\mathrm{P_S}$ parameters. The proper range of the values of those parameters depends on the characteristics of the interferences affecting the BCC. Since the 30–120 MHz band for BCC is usually allocated for TV and radio broadcasts, the interference signals are static in time. Although other wireless services such as cordless phone and walkie-talkie may use the BCC band, their communication time usually lasts longer than 10 s. Under these static interferences, selecting the $\mathrm{P_S}$ value close to 1 reduces the number of packet retransmissions. The hop period $\mathrm{T_H}$ of hundreds of μs and the channel update period $\mathrm{T_I}$ on the order of ms are needed because data loss due to the blank time at every frequency switching can be much saved to help throughput. Through a Matlab simulation modeling the BCC system with its possible interferences, $\mathrm{P_S}$, $\mathrm{T_I}$, and $\mathrm{T_H}$ are chosen as 0.9, 450 μs, and 100 ms, respectively. With those parameters, data throughput of 8 Mb/s can be achieved under 30 dB SIR.

III. Transceiver Circuits

A. Body-to-Front-End Interface

Conventional radios are mainly concerned with impedance matching with an antenna at the front-end to transfer the maximum power. However, the proposed BCC uses a single electrode instead of the antenna, and the capacitance between the electrode and the transceiver ground ranges from 50 fF to 300 fF. Therefore, the electrode can be regarded as an open circuit in the operating frequencies under 150 MHz. Fig. 6 shows the body-to-front-end interface for time-division duplex. In the RX mode, the two parallel capacitors of 20 pF and 13 pF are switched on, enabling the 3rd order LC low pass filter of 120 MHz cut-off frequency. It rejects out-of-band signals and noises with 60 dB/dec roll-off. The input impedance of the LNA is made low enough to minimize the size of the off-chip inductor. The inductance for the LC chebyshev filter is calculated as $\mathrm{L} = 1.33\ \mathrm{R_L}/(2\pi f_{3\mathrm{dB}})$ with $f_{3\mathrm{dB}}$ the cut-off frequency and $\mathrm{R_L}$ the load impedance. Since the low-cost chip inductors available for $f_{3\mathrm{dB}} = 120$ MHz usually are < 180 nH, the $\mathrm{R_L}$ should be less than 100 Ω. In addition, the input impedance lower than 100 Ω can remove the 60 Hz power-line noise coupled through human body by its high pass filtering. The on-resistance of the MOS switch is less than 30 Ω and it adds to the input referred noise by just 0.1 dB according to simulations. In the TX mode, the two switches and the LNA are turned off. Since the body channel communication is based on near-field capacitive coupling, the output voltage applied to the electrode should be as high as possible to secure the large received signal [13]. To reduce the power consumption at the TX while providing enough voltage swing, the load capacitance of the body driver is minimized by switching off the parallel capacitors and the LNA. The body driver consumes just 0.7 mW with 1.5 V swing with only the parasitic capacitors at its load.

The parallel combination of CS and CG stages in the LNA converts the single-ended signal from the single electrode to the differential signal (Fig. 7). A following differential pair balances the differential OP and ON by removing the remaining common mode signal. The CG stage provides the 100 Ω impedance to the band-select filter. During the transmit phase, the gate of M1 is pulled down to the ground and the LNA input becomes a high impedance node. The two-step gain control switch at the load resistors prevents the receiver saturation due to large interferences injected through the human body.

B. Direct-Switching FSK Modulator

Fig. 8 shows the typical structure for direct FSK modulation which many low power radios for WPAN have adopted [14]. It modulates the frequency directly by changing the control voltage of a VCO according to the input data. The phase locked

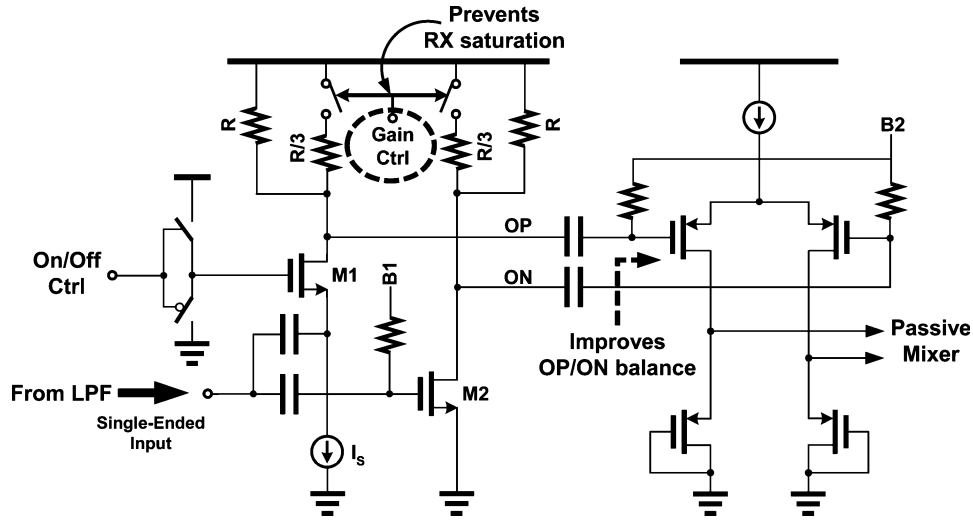

Fig. 7. Single-to-differential LNA.

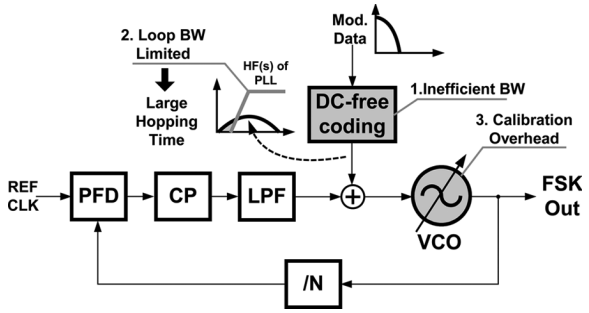

Fig. 8. Conventional direct FSK modulator.

loop prevents the frequency drift of the VCO during modulation. This structure is famous for its low power consumption and high speed modulation because it does not need an upconversion mixer and a DAC which consume a great portion of power [15]. And the loop bandwidth of the PLL does not limit the modulation speed because the modulating data is DC-free coded and its low frequency component attenuated by phase locking is negligible. However, it has many drawbacks for wideband frequency hopping system like the proposed BCC. First, most DC-free codes require twice the bandwidth of the NRZ code. This results in inefficient bandwidth utilization, increasing the SNR. Second, since the PLL rejects the low frequency signals on the VCO control line, the PLL loop bandwidth should be as low as possible to not disturb the power spectrum of the transmitted signal. Such a narrow loop bandwidth increases the band switching time of the AFH system severely. Even when the variable bandwidth scheme is applied to enhance the hopping speed, the switching time still amounts to over 12 μs [16]. Finally, the VCO nonlinearity due to the wide frequency range covered of 30–120 MHz requires complex calibration to guarantee accurate 10 MHz separation of the FSK signal.

Fig. 9(a) shows the proposed direct-switching modulator with two frequency synthesizers to overcome these difficulties. The internal PLLs generate two consecutive frequencies representing binary data and one of them is switched out to $\mathrm{FS_{OUT}}$. Unlike the conventional methods, the proposed modulator can change the frequency without disturbing the VCO control voltage or the division ratio of the PLL that alters its loop dynamics. Hence, the loop bandwidth can be as large as possible, minimizing the frequency switching time without degradation of the modulation speed. In addition, there is no need for DC-free coding of the data modulation and calibration of the VCO. Since the FSK is performed by direct-switching with < 500 ps delay, the target data rate of 10 Mb/s can be easily obtained. The divide-by-4 unit following the switch quadruples the internal frequency separation and thereby the reference frequency. The 4x reference clock reduces the PLL's band switching time by a factor of 4. The frequency division also compensates the phase noise and the reference spur increment due to the large loop bandwidth. Since the required frequency is under 120 MHz, power overhead due to the additional PLL can be controlled under 1 mW. Therefore, the 10 Mb/s FSK modulator with the hopping time of 4.2 μs consumes only 1.9 mW.

The output phases of the two integer-N PLLs using a common reference are aligned at every rising edge of the reference clock as shown in the waveform of Fig. 9(a). If these two signals are switched simultaneously at the synchronization edge, the phase continuity of the resulting FSK signal can be guaranteed. However, in the real implementation of the direct-switching modulator, the phase discontinuity may occur at its frequency changing moment because of the timing mismatch between the two PLL outputs. The timing mismatch mainly comes from the current mismatch in the charge pumps and the logic delay of the programmable dividers. In order to compensate for these, a fast-switching charge pump and a retiming flip-flop are designed in the frequency synthesizer as shown in Fig. 9(b). The cascode biasing is used in the charge pump to reduce the mismatch between the up and down currents when the $\mathrm{V_{ctrl}}$ changes. The $\mathrm{M_1}$ and $\mathrm{M_2}$ are added to improve the switching time by providing a discharge path for the pumping currents [17]. The flip-flop in the feedback path cancels the delay of the programmable divider by retiming the divided signal

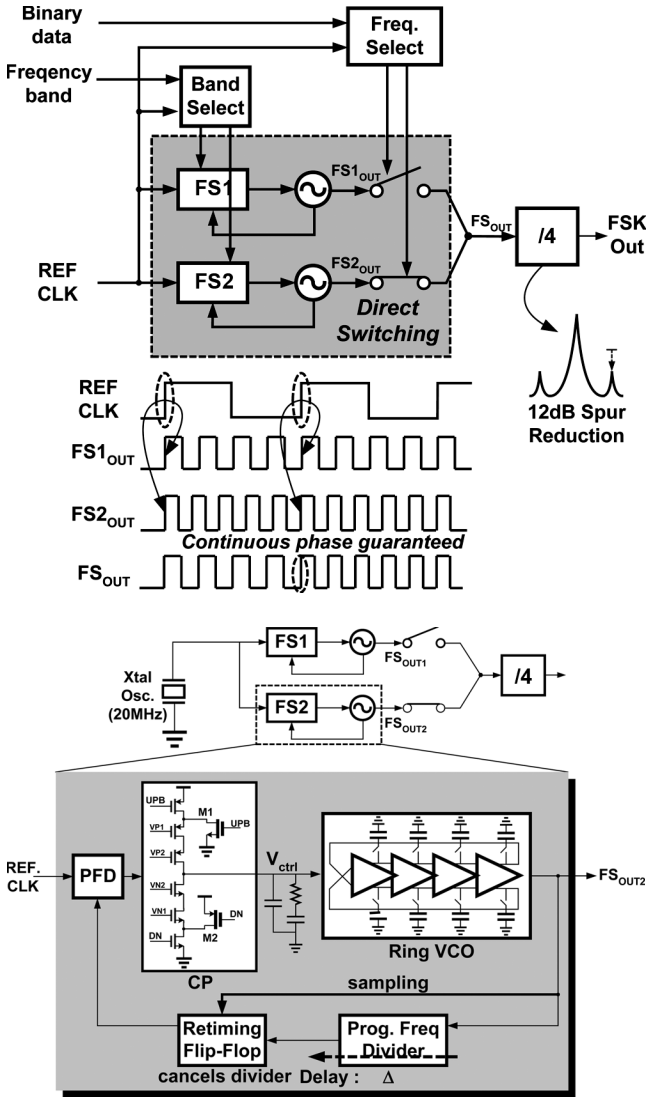

Fig. 9. (a) Direct-switching FSK modulator. (b) Internal frequency synthesizer.

with $\mathrm{FS_{OUT}}$. The spice simulation confirms that the timing mismatch between two PLLs is reduced to less than 50 ps under process variations. The ring-type VCO is chosen for its wide tuning range. To increase the tuning range further without degrading noise sensitivity, switching capacitors are placed on the intermediate nodes of the delay chain.

C. DLL-Based FSK Demodulator

Fig. 10 shows the spectrum of the 10 Mb/s BFSK signal with modulation index $(\mathrm{MI}) = 1$ after down-conversion to zero-IF. The binary data 1 and 0 correspond to $+5$ MHz and -5 MHz, respectively. The same magnitude and opposite sign of the two frequencies indicate that the transmitted data can be discriminated by rotating directions of I and Q signal in the phasor diagram. The black and gray arrows in Fig. 10 are the phasors representing I/Q channels which rotate clockwise or counterclockwise according to data. Projections of the I/Q phasors on the imaginary axis become the I/Q base band signals in time-domain. Although the original I/Q are analog signals, they are digitized by limiters and only the information of their polarity and zero-crossing is used for data detection. Conventionally, the demodulation method using flip-flops for lead/lag detection of the I and Q signals has been widely used for low cost FSK radios because of its simple implementation [18]. However, the zero-IF demodulator introduces large amount of jitter at every data transition originated from the zero crossing delay. Even though the rotating direction of the I/Q phasors reverses immediately after data transition, its detection has to be delayed to the next zero crossing of the I/Q signals, and the zero crossing delay is 50 ns in the worst case with a 5 MHz base band signal. The jitter effect gets serious as the MI of the FSK signal decreases. In this design, the MI value is 1, and the absolute jitter becomes larger than a half bit interval. To reduce the jitter, the proposed demodulator generates two additional signals, $\mathrm{I_D}$ and $\mathrm{Q_D}$ as shown in Fig. 11. These are $\pi/2$-delayed versions of the original I and Q signals. A delay-locked-loop is utilized to synthesize the accurate delay, and the control voltage of the internal VCDL is applied to the VCDL replicas. According to the phasor diagram, $\mathrm{I} \oplus \mathrm{Q_D}$ and $\overline{\mathrm{I_D} \oplus \mathrm{Q}}$ provide the received data with the zero crossing delay $< \pi/2$ (50 ns) while the minimum value of the two delays is always less than $< \pi/4$ (25 ns). The stacked inverter selects the output between $\mathrm{I} \oplus \mathrm{Q_D}$ and $\overline{\mathrm{I_D} \oplus \mathrm{Q}}$ for the shorter delay, so that the transition jitter is reduced by half. Two resistors and a capacitor at the output serve as a low pass filter which removes glitches due to the delay line mismatch and the frequency offset.

IV. Implementation Results

The body channel transceiver is designed and fabricated in 0.18 μm mixed mode CMOS process. Fig. 12 shows the chip microphotograph. The chip area is $2 \times 1.15\ \mathrm{mm}^2$ including pads. The symmetric blocks including the I/Q mixers, base band filters, and limiters in the RX and the dual frequency synthesizers in the TX are placed side by side to enhance the matching property of the circuit parameters such as gain, voltage offset, and time delay.

Fig. 13 shows the output spectrum of the local oscillator at the channel 2. Its phase noise is measured at -95 dBc/Hz @1 MHz and the reference spur is measured at -52 dBc. Without the divide-by-4 unit in the frequency synthesizer, the spur level would be raised to -40 dBc which is unacceptably high. For the other three channels, the measured data, summarized in the table in Fig. 13 show < 2 dB deviation. Fig. 14 shows the measured control voltages of the VCO in the PLL when frequency hopping happens. To search for the worst case hopping time, a random hopping sequence containing every case of the channel transition is applied. The channel hopping from channel 4 to channel 2 takes the longest hopping time, 4.2 μs which corresponds to 42 bit symbol in the maximum 10 Mb/s data rate. The hopping overhead decreases in proportion to the data rate. The measured 10 Mb/s BFSK spectrums of 4 different channels are superimposed as shown in Fig. 15. Since the dual frequency synthesizers are utilized, all signal spectrums are symmetric and identical over wide frequency range without any further calibration. Based on the results of the channel classifications, only the intact channels are used for communication. The time domain waveforms of the channel 1 confirm phase continuity of the FSK signal at the frequency switching moment thanks to

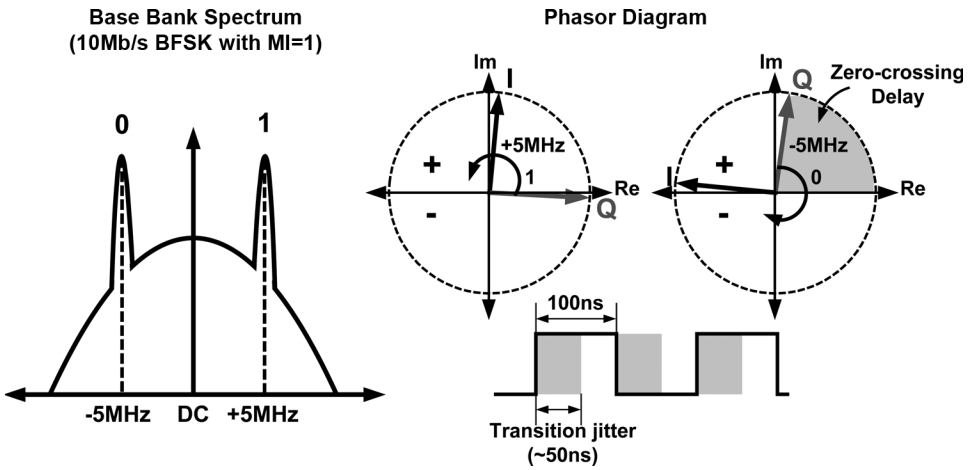

Fig. 10. Conventional zero-IF FSK demodulation.

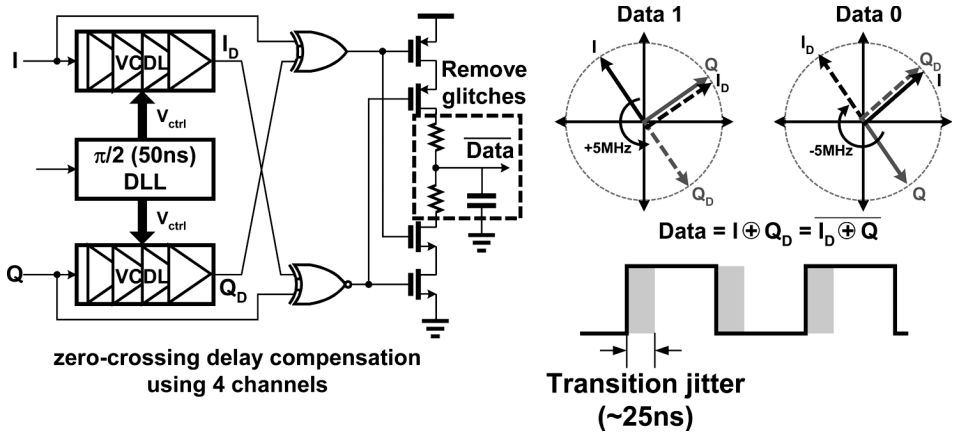

Fig. 11. DLL-based FSK demodulator.

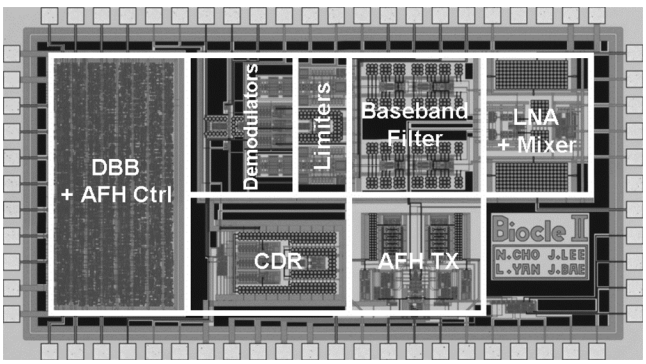

Fig. 12. Chip microphotograph.

the fast switching charge pump and the retiming flip-flop. The rectangular waveform of the modulator output generates odd order harmonics with 50% duty cycle. Unlike the other harmonics, the third-order harmonic of the channel1 is not easy to be filtered out because it overlaps with the channel4 spectrum (Fig. 15). However, since all transceivers in a BCC network use the same channel at the same time for time division multiple accessing, the spectral overlapping does not degrade communication quality. The demodulated bit stream in the RX side is shown in Fig. 16. For comparison, a conventional zero-IF demodulator is also designed and fabricated on the same chip [18], 2^7-1 PRBS is applied to the TX side to draw the eye diagrams. The upper waveform shows that the absolute jitter is reduced by 60% with the DLL-based demodulator. The proposed scheme can demodulate even 10 Mb/s data successfully. The absolute jitter is measured as 40 ns, which is larger than the estimated 25 ns. The 15 ns discrepancy may be caused by the inter symbol interferences due to base band filtering and the frequency offset. However, its cycle-to-cycle jitter is less than 10 ns, and the timing synchronization can be easily achieved with a simple open-loop CDR circuit.

The measurement setup of Fig. 17 is prepared to test the efficiency of interference rejection by the proposed AFH. A human subject attaches the TRX modules at his left and right hands with Ag/AgCl electrodes and stretched out his two arms. The TX module is powered by a battery to make external ground coupling. The RX module is connected to a Lab-Top computer through a serial cable. The spectrum analyzer measures the SIR level at the RX side. An RF signal generator emulates possible interferers to the body channel communication. The received BER is computed and displayed on a graph as a function of SIR. Fig. 18 shows the BER performance of the AFH BCC when a 100 kHz BW FM interference exists at 85 MHz. The received

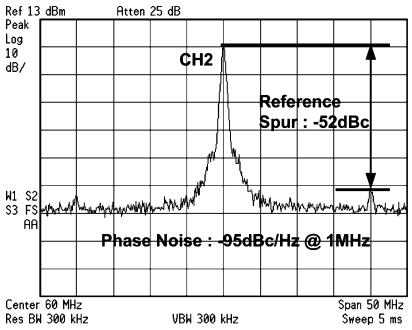

Measured LO Parameters in 4 Channels

CH	PN @ 1MHz	REF. Spur
1	-95dBc/Hz	-53dBc
2	-95dBc/Hz	-52dBc
3	-94dBc/Hz	-52dBc
4	-94dBc/Hz	-50dBc

Fig. 13. LO phase noise and reference spur.

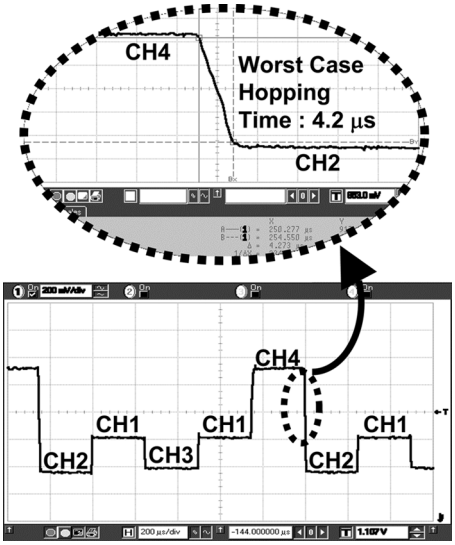

Fig. 14. Control voltage of the VCO at frequency hops.

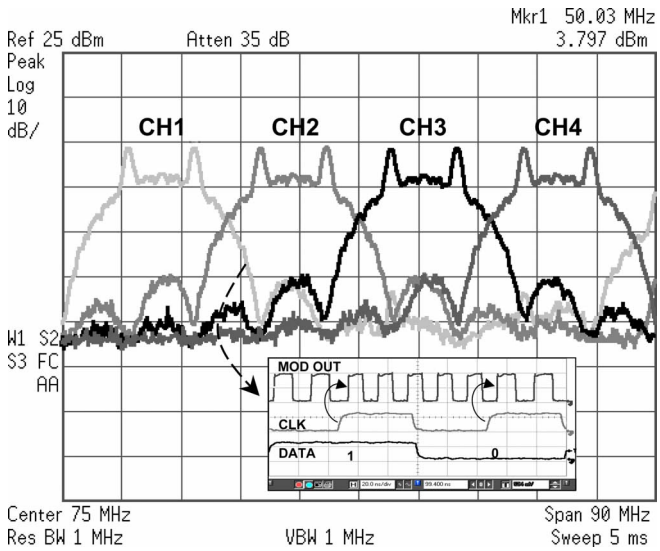

Fig. 15. Measured FSK spectrums for 4 channels.

signal power through the human subject is −45 dBm. For comparison, the normal frequency hopping and no hopping cases are also considered. Up to 10^{-5} BER, the AFH operates just like a normal FH. When the SIR decreases below 6 dB, the AFH controller detects that the channel 3 is corrupted, and abandons it in

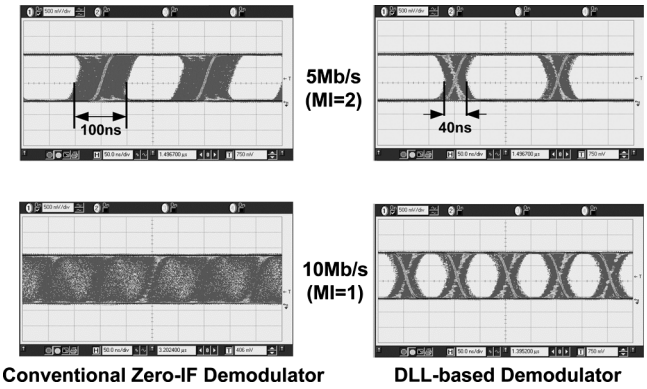

Fig. 16. Eye diagrams of the demodulated bit streams.

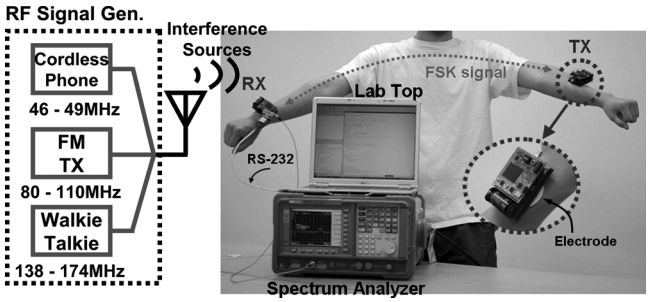

Fig. 17. Measurement setup testing interference rejection.

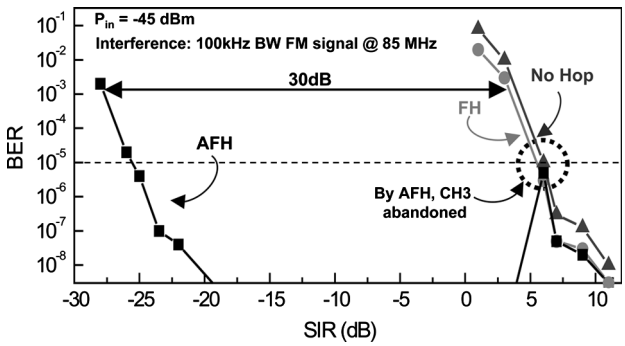

Fig. 18. BER performance of the AFH scheme.

the next hop. At this point, the BER drops abruptly. The BER of the AFH starts to increase again due to the LNA saturation, and the SIR level at 0.1% BER is −28 dB, which is a 30 dB improvement compared to the normal FH case. The performance summary in Table I shows that the proposed transceiver can support the scalability and the reliability required for body-area network [1]. From the on-body measurement, a successful communication is achieved over 1.8 m distance with −25 dBm noise interferences. Its BER at −62 dBm can be varied from 10^{-5} to 10^{-9} according to the required data rate. Table II compares the proposed transceiver with other short range radios. The data rate and BER of the body channel transceiver are highly scalable according to its applications. Thanks to the AFH, the interference rejection is 10 dB higher than the recent UWB transceiver [21]. The operating distance of the BCC is relatively short like 2 m, but enough to cover a body area network. In addition, since the BCC is confined to the body area, it does not interfere with adjacent networks [5]. Finally, the energy efficiency of the

TABLE I
PERFORMANCE SUMMARY

Frequency Band		30 MHz - 120 MHz
Modulation		Adaptive Frequency Hopping FSK
Front - End Voltage Gain		36.1 dB / 25.8 dB
Sensitivity		-65 dBm
1-dB Compression Point		-40 dBm / -28.5 dBm
SIR @ 10^{-3} BER		-28 dB
Input Impedance		100 Ohm
LO Phase Noise		-95 dBc/Hz @ 1 MHz offset
Operating distance		> 1.8 m @ -25 dBm interference
Hopping Overhead (Blank Time)		4.2 μs
Data Rate		10 Mb/s - 60 kb/s
BER @ -62 dBm		10^{-5} @ 10Mb/s / <10^{-9} @ 60kb/s
Supply Voltage		1.0 V / 1.5 V for Body Driver
Power Consumption	RX	2.25 mW
	TX	0.9 mW
	Frequency Synthesizer	0.95 mW
	Digital Block	0.5 mW
Energy/bit		0.37 nJ/b

TABLE II
PERFORMANCE COMPARISON WITH CONVENTIONAL SHORT-RANGE RADIOS

Parameters	B. W. Cook '06 ref. [19]	W. Kluge '06 ref. [20]	F.S. Lee '07 ref. [21]	This Work
Data Rate BER Scalability	500kb/s Fixed BER	250kb/s Fixed BER	16Mbps-10kbps Fixed BER	10Mbps-60kbps Scalable BER
Frequency Band	2.4GHz	2.4GHz	3 - 5GHz	30 - 120MHz
SIR @ 10^{-3} BER	NA	NA	-15dB	-28dB (10dB ▼)
Network Coverage	20m	15m	10m	2m
Path Loss/Distance on a Body	50 - 70 dB/dec	50 - 70 dB/dec	50 - 70 dB/dec	25 dB/dec
Energy/bit	3nJ/b	130nJ/b	2.5nJ/b	0.37nJ/b (1/7)

TABLE III
PERFORMANCE COMPARISON WITH CONVENTIONAL BODY CHANNEL TRANSCEIVERS

Parameters	M. Shinagawa '07 ref. [4]	S.J. Song '06 ref. [6]	S.J. Song '07 ref. [7]	This Work
Modulation	No	No	3-Level PPM	AFH FSK
Frequency Band	0 - 10MHz	1 - 100MHz	15 - 60MHz	30 - 120MHz
Sensitivity	NA	-35dBm	-40dBm	-65dBm
SIR @ 10^{-3} BER	NA	>15dB	>15dB	-28dB
Energy/bit	65nJ/b	2.5nJ/b	0.23nJ/b	0.37nJ/b

body channel transceiver is 7 times better than other works. This low energy is possible because of the low path loss of the body channel and the low frequency operation of the transceiver. The performance comparison with the conventional body channel transceiver is summarized in Table III. Although the energy consumption of the proposed transceiver is slightly larger, the sensitivity and the robustness to the in-band interferences are greatly improved.

V. CONCLUSION

An interference resilient, 60 kb/s–10 Mb/s body channel transceiver for body area network is proposed. The transceiver uses the human body as a signal transmission medium in the 30–120 MHz frequency range for energy-efficient and scalable data communication around the body. In the frequency range of BCC, the human body may operate as a receiving antenna and pick-up large interferences to the body channel RX, degrading its SIR to -22 dB. In order to avoid the body-induced interferences, an AFH scheme that monitors channel status continuously and selects only the clean channels is introduced to BCC. To support 10 Mb/s wideband FSK signaling with the fast AFH, the direct-switching modulator and the DLL-based demodulator are incorporated in the transceiver design. The dual frequency synthesizers in the modulator reduce the frequency hopping overhead to 4.2 μs without degradation of the phase noise and the reference spur. As a result, the AFH body channel transceiver can withstand -28 dB SIR with $< 10^{-3}$ BER and its energy consumption is 0.37 nJ/b. Finally, > 1.8 m operating distance is measured with -65 dBm RX sensitivity.

REFERENCES

[1] *Body Area Networks (BAN)*, IEEE 802.15 WPAN™ Task Group 6, Nov. 2007 [Online]. Available: http://www.ieee802.org/15/pub/TG6.html

[2] A. Fort, J. Ryckaert, C. Desset, P. D. Doncker, P. Wambacq, and L. V. Biesen, "Ultra-wideband channel model for communication around the human body," *IEEE J. Sel. Areas Commun.*, vol. 24, no. 4, pp. 927–933, Apr. 2006.

[3] T. Zasowski, F. Althaus, M. Stager, A. Wittneben, and G. Troster, "UWB for noninvasive wireless body area networks: Channel measurements and results," in *IEEE Conf. Ultra Wideband Systems and Technologies*, Nov. 2003, pp. 285–289.

[4] M. Shinagawa, M. Fukumoto, K. Ochiai, and H. Kyuragi, "A near-field-sensing transceiver for intrabody communication based on the electrooptic effect," *IEEE Trans. Instrum. Meas.*, vol. 53, pp. 1533–1538, Dec. 2004.

[5] N. Cho, J. Yoo, S.-J. Song, J. Lee, S. Jeon, and H.-J. Yoo, "Human body characteristics as a signal transmission medium for intrabody communication," *IEEE Trans. Microw. Theory Tech.*, vol. 55, no. 5, pp. 1080–1086, May 2007.

[6] S.-J. Song, N. Cho, and H.-J. Yoo, "A 0.2-mW 2-Mb/s digital transceiver based on wideband signaling for human body communications," *IEEE J. Solid-State Circuits*, vol. 42, no. 9, pp. 2021–2033, Sep. 2007.

[7] S.-J. Song, N. Cho, S. Kim, J. Yoo, S. Choi, and H.-J. Yoo, "A 0.9 V 2.6 mW body-coupled scalable PHY transceiver for body sensor applications," in *IEEE Int. Solid-State Circuits Conf. Dig. Tech. Papers*, Feb. 2007, pp. 366–367.

[8] P. J. Dimbylow, "FDTD calculations of the whole-body averaged SAR in an anatomically realistic voxel model of the human body from 1 MHz to 1 GHz," *Phys. Med. Biol.*, vol. 42, pp. 479–490, 1997.

[9] S. Gabriel, R. W. Lau, and C. Gabriel, "The dielectric properties of biological tissues: II. Measurement in the frequency range 10 Hz to 20 GHz," *Phys. Med. Biol.*, pp. 2251–2269, Nov. 1996.

[10] P. Popovski, H. Yomo, and R. Prasad, "Strategies for adaptive frequency hopping in the unlicensed bands," *IEEE Wireless Commun.*, vol. 13, pp. 60–67, Dec. 2006.

[11] B. Sklar, *Digital Communications : Fundamentals and Applications*, 2nd ed. Upper Saddle River, NJ: Prentice Hall PTR, 2001.

[12] Y.-H. You, C.-H. Park, M.-C. Ju, K.-W. Kwon, and J.-W. Cho, "Adaptive frequency hopping scheme for interference-limited WPAN applications," *Electron. Lett.*, vol. 37, no. 15, pp. 976–978, Jul. 2001.

[13] T. G. Zimmerman, "Personal area network: Near-field intra body communication," *IBM Syst. J.*, vol. 35, no. 3–4, pp. 609–617, 1996.

[14] T. Cho *et al.*, "A single-chip CMOS direct-conversion transceiver for 900 MHz spread-spectrum digital cordless phones," in *IEEE Int. Solid-State Circuits Conf. Dig. Tech. Papers*, Feb. 1999, pp. 228–229.

[15] P. V. Zeijl *et al.*, "A Bluetooth radio in 0.18 μm CMOS," *IEEE J. Solid-State Circuits*, vol. 37, no. 12, pp. 1679–1687, Dec. 2002.

[16] C.-Y. Yang and S.-I. Liu, "Fast-switching frequency synthesizer with a discriminator-aided phase detector," *IEEE J. Solid-State Circuits*, vol. 35, no. 10, pp. 1445–1452, Oct. 2000.
[17] M. Demirkan and R. R. Spencer, "A 1.8 Gpulses/s UWB transmitter in 90 nm CMOS," in *IEEE Int. Solid-State Circuits Conf. Dig. Tech. Papers*, Feb. 2008, pp. 116–117.
[18] G. Ahlbom, L. Egnell, and C. Wickman, "Digital demodulator for optical FSK signals," *Electron. Lett.*, vol. 26, no. 5, pp. 290–292, Mar. 1990.
[19] B. W. Cook, A. D. Berny, A. Molnar, S. Lanzisera, and K. S. J. Pister, "An ultra-low power 2.4 GHz RF transceiver for wireless sensor networks in 0.13 μm CMOS with 400 mV supply and an integrated passive RX front-end," in *IEEE Int. Solid-State Circuits Conf. Dig. Tech. Papers*, Feb. 2006, pp. 370–371.
[20] W. Kluge, F. Poegel, H. Roller, M. Lange, T. Ferchland, L. Dathe, and D. Eggert, "A fully integrated 2.4 GHz IEEE 802.15.4 compiant transceiver for Zigbee applications," in *IEEE Int. Solid-State Circuits Conf. Dig. Tech. Papers*, Feb. 2006, pp. 372–373.
[21] F. S. Lee and A. P. Chandrakasan, "A 2.5 nJ/b 0.65 V 3-to-5 GHz subbanded UWB receiver in 90 nm CMOS," in *IEEE Int. Solid-State Circuits Conf. Dig. Tech. Papers*, Feb. 2007, pp. 116–117.

Namjun Cho (S'04) received the B.S. (*summa cum laude*) and M.S. degrees from KAIST, Daejeon, Korea, in 2004 and 2006, respectively. He is currently working toward the Ph.D. degree at KAIST.

He has worked on developing UHF RFID tag chip integrated with environmental monitoring sensors and low-power digital-to-analog converters for hearing aid systems. His current research interests include low-power biomedical microsystems and the wireless transceivers for communication among wearable and implantable health care devices.

Long Yan (S'07) received the B.S. degree in electrical engineering and computer science from KAIST, Daejeon, Korea, in 2007. He is currently working toward the M.S. degree in electrical engineering and computer science at KAIST.

He has worked on developing a low-power transmitter chip for body channel communication. His current research interests include wirelessly powered biomedical sensor design for body area networks.

Joonsung Bae (S'07) received the B.S. degree in electrical engineering and computer science from KAIST, Daejeon, Korea, in 2007. He is currently working toward the M.S. degree in electrical engineering and computer science at KAIST.

His current research interests include high-speed and low-energy on-chip global interconnects and low-power CMOS transceiver design for body area networks.

Hoi-Jun Yoo (M'95–SM'04–F'08) graduated from the Electronic Department of Seoul National University, Seoul, Korea, in 1983 and received the M.S. and Ph.D. degrees in electrical engineering from the Korea Advanced Institute of Science and Technology (KAIST), Daejeon, Korea, in 1985 and 1988, respectively. His Ph.D. work concerned the fabrication process for GaAs vertical optoelectronic integrated circuits.

From 1988 to 1990, he was with Bell Communications Research, Red Bank, NJ, where he invented the two-dimensional phase-locked VCSEL array, the front-surface-emitting laser, and the high-speed lateral HBT. In 1991, he became a manager of the DRAM design group at Hyundai Electronics and designed a family of fast-1M DRAMs to 256M synchronous DRAMs. In 1998, he joined the faculty of the Department of Electrical Engineering at KAIST and now is a full professor. From 2001 to 2005, he was the director of System Integration and IP Authoring Research Center (SIPAC), funded by Korean Government to promote worldwide IP authoring and its SOC application. From 2003 to 2005, he was the full time Advisor to Minister of Korea Ministry of Information and Communication and National Project Manager for SoC and Computer. In 2007, he founded System Design Innovation & Application Research Center (SDIA) at KAIST to research and to develop SoCs for intelligent robots, wearable computers and bio systems. His current interests are high-speed and low-power Network on Chips, 3D graphics, Body Area Networks, biomedical devices and circuits, and memory circuits and systems. He is the author of the books *DRAM Design* (Seoul, Korea: Hongleung, 1996; in Korean), *High Performance DRAM* (Seoul, Korea: Sigma, 1999; in Korean), *Low-Power NoC for High-Performance SoC Design* (CRC Press, 2008), and chapters of *Networks on Chips* (New York, Morgan Kaufmann, 2006).

Dr. Yoo received the Electronic Industrial Association of Korea Award for his contribution to DRAM technology in 1994, the Hynix Development Award in 1995, the Design Award of ASP-DAC in 2001, the Korea Semiconductor Industry Association Award in 2002, the KAIST Best Research Award in 2007, and the Asian Solid-State Circuits Conference (A-SSCC) Outstanding Design Awards in 2005, 2006 and 2007. He is an IEEE fellow and serving as an Executive Committee Member and the Far East Secretary for IEEE ISSCC, and a Steering Committee Member of IEEE A-SSCC. He was the Technical Program Committee Chair of A-SSCC 2008.